

Article

Modeling and Loading Effect of Wind on Long-Span Cross-Rope Suspended Overhead Line with Suspension Insulator

Qixin Qin ¹, Xi Tu ^{1,2}, Yujing Hu ^{1,3}, Zhisong Wang ^{1,2,*}, Lin Yu ⁴ and Shengli Hou ⁴

- ¹ College of Civil Engineering, Chongqing University, Chongqing 400044, China; tuxi@cqu.edu.cn (X.T.)
² Key Laboratory of New Technology for Construction of Cities in Mountain Area, Chongqing University, Ministry of Education, Chongqing 400045, China
³ Design Institute of Chongqing Iron & Steel Group Co., Ltd., Chongqing 400084, China
⁴ Chongqing Haizhuang Wind Power Engineering Technology Co., Ltd., Chongqing 401258, China; hzgcjszx@163.com (S.H.)
* Correspondence: wangzhisong@cqu.edu.cn

Abstract: The long-span Cross-Rope Suspended (CRS) system is composed of a transmission line (conductor), a long-span suspension cable, and an insulator. The previously introduced long-span CRS with a Tension Insulator (CRSTI) has shown applicability in mountainous areas. However, the tension insulator divided the suspension cable into several sections, which made the construction of a long-span CRS rather difficult. This paper introduces long-span CRS with a Suspension Insulator (CRSSI), in which the suspension cable was not disconnected, and the conductor was supported by a suspension insulator connected to the suspension cable. For the purposes of assessment, the initial shape of the suspension cable with concentrated loading from the self-gravity of the suspension insulator and the conductors was studied, and practical lengths in construction could be calculated exactly. Secondly, the structural performance of CRSSI, including its dynamic properties and the loading effect of wind, was discussed by means of numerical analysis. Vibration modes of the structure were obtained by FE analysis. Finally, structural deformation under static wind loading was studied. The result of the analysis showed that the stiffness of CRSSI was lower than CRSTI. The first frequency of CRSSI was 6% smaller than CRSTI. Regarding static wind loading, additional displacement of the insulator contributed to the maximum displacement of long-span CRSSI. Apparently, the displacement of the suspension insulator increased with wind speed. Moreover, the number of spans has an insignificant influence on tension force and deformation.

Keywords: cross-rope suspension; dynamics; long span; power transmission line; suspension insulator; wind load; finite element analysis; geometric nonlinear



Citation: Qin, Q.; Tu, X.; Hu, Y.; Wang, Z.; Yu, L.; Hou, S. Modeling and Loading Effect of Wind on Long-Span Cross-Rope Suspended Overhead Line with Suspension Insulator. *Buildings* **2024**, *14*, 656. <https://doi.org/10.3390/buildings14030656>

Academic Editor: Giuseppina Uva

Received: 18 December 2023

Revised: 18 January 2024

Accepted: 1 February 2024

Published: 1 March 2024



Copyright: © 2024 by the authors. Licensee MDPI, Basel, Switzerland. This article is an open access article distributed under the terms and conditions of the Creative Commons Attribution (CC BY) license (<https://creativecommons.org/licenses/by/4.0/>).

1. Introduction

Long-span Cross-Rope Suspended (CRS) overhead lines are a type of structure in which the transmission line is supported by a long-span suspension cable. They are suitable in mountainous areas. Compared with conventional CRS, steel pylons are removed, and the span of the cross-rope increases to hundreds of meters. Generally, both ends of the cross-rope, also called a suspension cable, are directly fixed on top of mountains.

The first long-span CRS structure was reported in Cape Town, South Africa, in 2011: it was called the “invisible tower line”, and it provided better protection of the local landscape [1]. Cross-Rope Suspended systems with a Tension Insulator (CRSTI) (Figure 1) are currently the adopted type of CRS. For CRSTI, a Tension Insulator (TI) connects multiple sections of suspension cable and becomes a key member of the structure. Thus, the transmission line is directly supported by a suspension cable. Li [2] established a finite element model for CRSTI, which was used to analyze the dynamic characteristics and study the wind-induced response. The horizontal displacements and tension force of the suspension cables of CRSTI increased with the increase in wind speed. These results provide

a basis for the practical engineering design of CRSTI. Tu [3] studied the corresponding vortex-induced vibration and the controlling methods of CRSTI by numerical simulation. However, due to the huge tension force, high tensional mechanical capacity is required for TI, which results in difficulty in construction and relatively poor economic efficiency. Therefore, a new type of CRS system is proposed, which is CRS with a Suspension Insulator (CRSSI) (Figure 2).

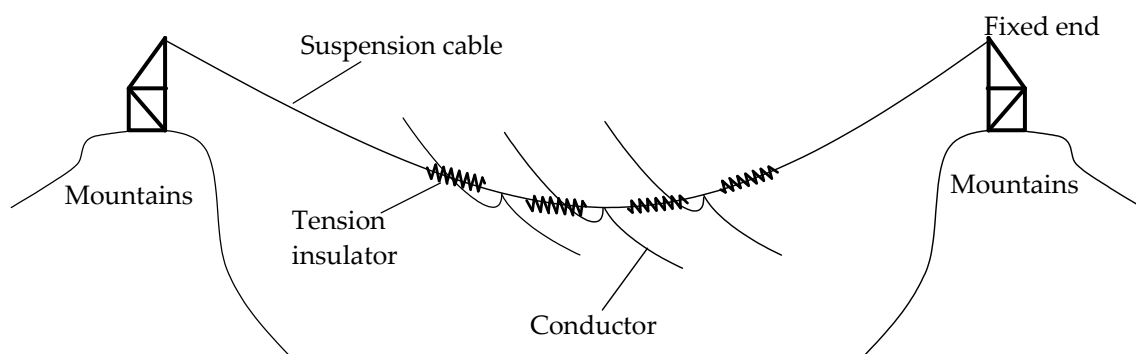


Figure 1. Long-span Cross-Rope Suspension overhead transmission line with Tension Insulator.

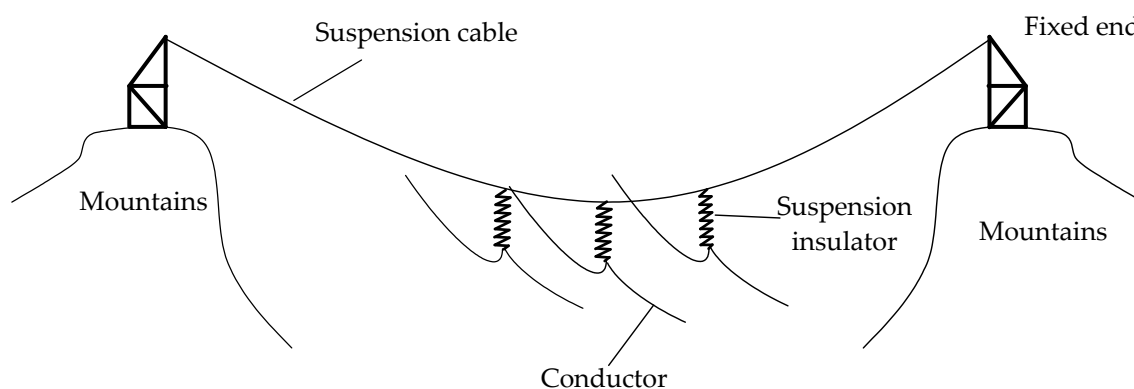


Figure 2. Long-span Cross-Rope Suspension overhead transmission line with Suspension Insulator.

For CRSSI, the upper end of the Suspension Insulator (SI) is hung on a suspension cable, and the lower end is connected to the conductor. Thus, the weight load of the transmission line is directly subject to the insulator. The structure for CRSSI is simpler than CRSTI, and construction is easier. Additionally, the investment of CRSSI is less than that of CRSTI. Obviously, the wind-induced response is smaller in CRSTI compared with CRSSI. Simultaneously, the initial configuration of the suspension cable differs from that of CRSTI. Therefore, it is necessary to determine the function of the suspension cable in order to calculate its length accurately during practical construction. To select the appropriate type for CRS construction, a thorough investigation into CRSSI and a comparison between CRSSI and CRSTI were essential.

Currently, the Finite Element Method (FEM) has been widely adopted for analyzing complex flexible structures with large geometric deformations, which is applicable for long-span CRS as well [4]. The basis of the analysis for CRS systems with large spans is the initial shape of the conductors and suspension cables. Based on the traditional shape-finding method for cables, Jia and Liu [5] introduced a method of finding the initial shape of overhead transmission lines. Peyrot [6] proposed a method for structural analysis of cable using nonlinear elastic suspended catenary units and presented the results of static analysis of 500 kV cable tower transmission lines. Nie [7] modeled a guyed tower with different element types based on finite element analysis and compared the influence of different models on the overall response. Kempner [8] studied the dynamic characteristics

of a guyed tower and proposed an analysis method for structural modal and vibrations. McClure [9] studied the case of a line section experiencing two tower failures that were caused by conductor breakages during an ice storm and established a macroscopic modeling approach to dynamic analysis. Wang [10] established a finite model for a V-type insulator string under dynamic wind load and compared dynamic and static calculation results. Duan [11] investigated the aerodynamic coefficients of the contact line with two levels of wear under different wind angles by means of the nonlinear finite element model and summarized the effect of a damping dropper. Zhang [12] developed a finite model to estimate the load-bearing capacity of a transmission tower and explained the reason for the failure modes and the difference in buckled members using dynamic analysis and static analysis. Zhang [13] established a design tool with a three-degrees-of-freedom hybrid model that accommodated interactions of vertical, horizontal, and torsional movements. Desai [14] developed a three-node, isoparametric cable element with three translationals and a torsional degree of freedom at each node to obtain the envelope of galloping. Eric [15] explained models for time histories of wind velocities of transient tornadoes and microburst events and performed dynamic structural analysis of the two events.

This type of structure is sensitive to wind load, and the structural displacements caused by wind loads are important to be concerned with [16–18]. For large-span wind-sensitive structures such as cable-supported transmission line systems, vortex-induced vibration caused by uniform flow is the most typical form of vibration and has been the focus of researchers' attention [19]. Jafari [20] summarized different sources of wind-induced cable vibration, consisting of vortex-induced vibration, rain-wind-induced vibration, dry galloping, ice galloping, and wake galloping. Martins [21] investigated the application of optimization techniques to cable-stayed bridges, which showed that bridges with innovative cable arrangements like crossing cables attracted the interest of researchers. Liu [22] summarized the current state of research on pantograph–catenary interaction for high-speed railways and proposed future directions for improving the system to ensure optimal performance at speeds of 400 km/h and above. Yin [23] proposed a filtering method for abnormal working conditions based on density clustering to solve the problem of deviation in the wind vane in wind turbines. Okamura [24] pointed out that the blow-down angle was also important in a wind response analysis of a transmission tower in a mountainous area. For a mountainous area, the combination of wind and ice in extreme conditions has a significant impact on the design load of CRS. Keyhan [25] proposed a new method for determining wind loads on conductors based on fluid–solid coupling analysis. Lalonde [26] carried out a study of Aluminum Conductor Steel Reinforcement (ACSR) under wind-induced loading using the finite element method and compared it with experimental data. Jia [27] compared the fatigue calculation results with those obtained from a linear stochastic dynamic analysis in the frequency domain and certified that wind-induced fatigue calculation procedures were widely adopted in various types of structures. Deng [28] presented a four-span transmission line system subjected to skew incident wind forces on a lattice suspension tower via experimental and numerical approaches. Pombo [29,30] addressed the influence of track and environmental conditions on the pantograph–catenary, and results were obtained for high-speed trains running at 300 km/h in relation to the separation between pantographs. Stickland [31] measured a damped oscillation of a section of the UK East Coast Main Line catenary and increased mechanical damping, which was found to raise the mechanical damping coefficient. Song [32] characterized pointwise stochastics of Contact Wire Irregularity (CWI) and introduced the power spectral density (PSD) function for CWI.

This paper discussed the expression of the initial shape of cable under the action of a single concentrated force. A finite element model was established to analyze the dynamic characteristics of CRSSI. Analysis of static wind loads on the CRSSI was carried out. Furthermore, the response of the static wind load for CRSSI was compared with that of CRSTI, offering a foundational theory for the selection of CRS and practical engineering construction.

2. Initial Shape of Cross-Rope under Loading of Conductors

In the CRS system, the initial shape of the cable is meaningful to provide an unstressed length of cable and final shape after construction. As known, the catenary is the initial shape of cable with only self-weight and no additional loading. However, the initial shape of the cable changes when the additional loading of the self-weight for conductor and insulators is considered. In this chapter, the functions of the cable without loading and with additional loading were derived, which is the basis for further FE modeling.

2.1. Approximate Equation of Catenary of Suspension Cable

Without additional external vertical loading and considering only self-weight, the catenary is the initial shape of the cable fixed on both ends. For long-span CRS, the height of both ends of the suspension cable varies due to terrain. Therefore, the shape of a cable with unequal altitude and its derivation are studied in this chapter. A catenary with unequal height is shown in Figure 3. In this figure, point A denotes the left end, and point B denotes the right end. A small element of suspension cable composed of two ends of *i* and *j* was taken as follows (shown in Figure 4).

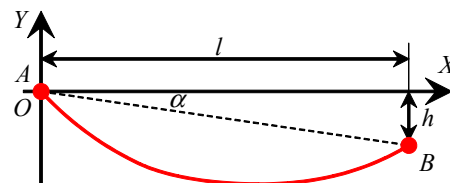


Figure 3. Catenary with unequal height at both ends.

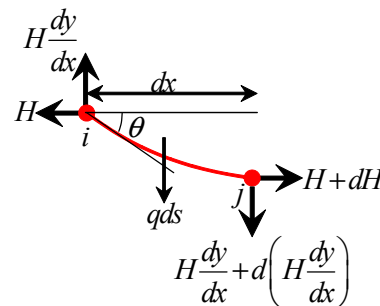


Figure 4. Calculation diagram of a catenary with unequal height at both ends.

Both ends of the element were subjected to tension along the tangential direction, which was decomposed into horizontal and vertical directions, respectively. Moreover, the element was subjected to distributed loads caused by its self-weight. The equilibrium equations of the element are as follows:

$$H + dH - H = 0 \tag{1}$$

$$H \frac{dy}{dx} + d\left(H \frac{dy}{dx}\right) - H \frac{dy}{dx} + qds = 0 \tag{2}$$

where *q* is the mass of the unit length of the cable.

According to Equation (1), the horizontal component of the cable force, *H*, is constant along the cable. According to Equation (2), the differential equation of the cable is rewritten as follows:

$$\frac{d^2y}{dx^2} = -\frac{1}{H} \frac{qds}{dx} \tag{3}$$

The differential formula of arc length gave the following:

$$ds = \sqrt{1 + \left(\frac{dy}{dx}\right)^2} dx \quad (4)$$

Based on Equations (3) and (4), the differential formula of catenary of cable gave

$$\frac{d^2y}{dx^2} = -\frac{q}{H} \sqrt{1 + \left(\frac{dy}{dx}\right)^2} \quad (5)$$

Assuming that the self-weight load q was constant along the cable, parameter c was defined as

$$c = -\frac{q}{H} \quad (6)$$

Substituting c in Equation (6) into Equation (5) and integrating, the expression of cable produced the following:

$$y = \frac{1}{c} \cosh(cx + a) + b \quad (7)$$

Boundary conditions were given:

$$\begin{cases} x = 0, y = 0 \\ x = l, y = h \end{cases} \quad (8)$$

Based on Equations (7) and (8), a and b were solved:

$$a = \operatorname{arcsinh} \left[\frac{hc}{2\sinh\left(\frac{cl}{2}\right)} \right] \quad (9)$$

$$b = -\frac{1}{c} \cosh a \quad (10)$$

The initial shape of the cable considering only self-weight was calculated using the above formula, which served as the initial base for the following analysis.

Also, the sag of the suspension cable was calculated by Equation (11), in which x was half of one span for a conductor.

$$y_{\text{sag}} = \frac{1}{c} \cosh(cx_{0.5\text{span}} + a) + b \quad (11)$$

2.2. Approximate Equations of Suspension Cable under the Action of Single Concentrated Force

In long-span CRSSI, the expression for the cable differed from the above calculation due to the additional loading caused by SI and conductors. For simplification, additional concentrated force was set at the lowest point of the catenary, and the cable was symmetrical in shape. The demonstration of loading on cable is shown in Figure 5, where m denotes the sum of the mass of conductors and the mass of the insulator. In Figure 5, point A denotes the left end, point B denotes the right end, and point C denotes the lowest point.

According to the differential equations of cable mechanics in the above chapter, despite the additional loading from the conductor and the overhanging insulator, the cable between the fixed end and SI kept the original shape of the catenary. Therefore, in order to derive the shape formula of cable considering the concentrated force, half of the mass of conductors and insulator, m_2 , was transformed into an equivalent cable segment with length x , as shown in Figure 6. Point A denotes the fixed end. Point B denotes the lowest end of the cable and the starting point of the equivalent cable. Point C denotes the end of the equivalent cable. The dashed line denotes the symmetric part of the cable from the fixed end, $A(0, 0)$, to the hanging point, $B(x_0, y_0)$. The red line segment from B to C denotes the equivalent cable for

the mass of conductors and the insulator. Point C denotes the virtual lowest point of the equivalent catenary. Accordingly, A, B, and C were located in the same catenary.

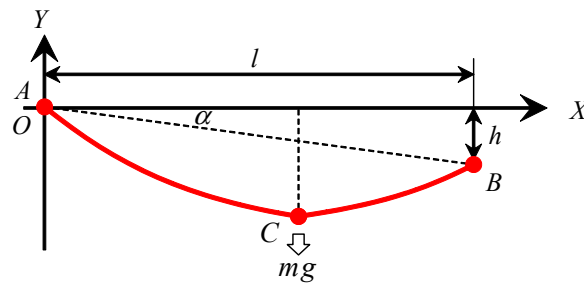


Figure 5. Diagram of the force considering the mass of the conductor and the SI.

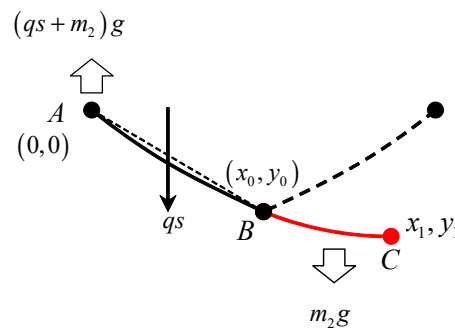


Figure 6. Calculation diagram considering the equivalent cable segment.

The base of the differential formula of the arc length is as follows:

$$ds = \sqrt{1 + \left(\frac{dy}{dx}\right)^2} dx \tag{12}$$

$$s = \int_0^l \sqrt{1 + \left(\frac{dy}{dx}\right)^2} dx \tag{13}$$

The equivalent length l_e of the virtual suspension cable is given by the mass of the conductors and insulator:

$$l_e = \frac{m_2 g}{q} \tag{14}$$

Replacing s in Equation (13) with l_e in Equation (14) yields

$$\frac{m_2 g}{q} = \int_{x_0}^{x_1} \sqrt{1 + \left(\frac{dy}{dx}\right)^2} dx \tag{15}$$

According to the formula of catenary,

$$\frac{dy}{dx} = \sinh(cx + a) \tag{16}$$

Replacing dy/dx in Equation (15) with Equation (16), the catenary of suspension cable is given as follows:

$$\frac{m_2 g}{q} = \int_{x_0}^{x_1} \sqrt{1 + (\sinh(cx + a))^2} dx \tag{17}$$

Based on Equations (9) and (17), the coordinate x_0 of the equivalent suspension length can be solved. Bringing x_0 into Equation (7), y_0 is obtained.

According to the geometric relationship,

$$y_f = f(x + x_0) - y_0 \quad (18)$$

Bringing x_0 and y_0 into Equation (18), the shape of cable under the concentrated force is obtained. The above formula took the lowest point of the catenary as the origin.

2.3. Numerical Solution of the Approximate Equations for Cables under the Action of Concentrated Forces

In practical engineering, it is possible to carry out an analysis of the numerical solution of the function using design conditions so that the initial shape and the initial prestress can be defined for construction.

We can assume that the expression of the catenary is as follows:

$$y = a \cosh\left(\frac{x - b}{a}\right) - c \quad (19)$$

where a , b , and c are unknown parameters for the above equation.

The origin, the lowest point, and the end point of the suspension cable in the practical project were set according to the actual topography. The origin was $A(0, 0)$, and the lowest point was $B(x_0, y_0)$. In the above analysis, it was found that the tangent line at the end point C was horizontal, and the mass and length of the equivalent suspension section can be obtained via calculation.

We can bring $A(0, 0)$ into Equation (19):

$$c = a \cosh\left(\frac{-b}{a}\right) \quad (20)$$

Replacing c in Equation (19) by Equation (20), the expression was simplified:

$$y = a \cosh\left(\frac{x - b}{a}\right) - a \cosh\left(\frac{-b}{a}\right) \quad (21)$$

We can bring $B(x_0, y_0)$ into Equation (21):

$$0 = a \cosh\left(\frac{x_0 - b}{a}\right) - a \cosh\left(\frac{-b}{a}\right) - y_0 \quad (22)$$

According to Equation (22), a and b were solved by a calculation process. First, the initial values of a , b were selected and were brought into Equation (23):

$$\Delta_b = y_0 - \left(a \cosh\left(\frac{x_0 - b}{a}\right) - a \cosh\left(\frac{-b}{a}\right) \right) \quad (23)$$

If $\Delta_b = 0$, the value of b is satisfied. For simplification, the thresholding value for Δ_b was given:

$$-0.001 < \Delta_b < 0.001 \quad (24)$$

If Equation (24) was satisfied, the value of b was satisfied. If not, the value of b was changed to recalculate. This process continued until the best value of b was determined. The function of the cable was given by a and b .

The calculation of the length of the arc was given:

$$s = \int_{x_0}^{x_1} \sqrt{1 + y'^2} dx \quad (25)$$

According to Equation (25), the length of the suspension cable from B to C can be calculated by Equation (25), where C is a random point in the suspension cable. The length

l_{bc} from B to C can be compared with the equivalent section length l_e , which was defined as Equation (14). As per the analysis above, it was accurate when $l_{bc} = l_e$. For simplification, the thresholding number for l_{bc} was given as follows:

$$-0.001 < \frac{l_{bc} - l_e}{l_{bc}} < 0.001 \quad (26)$$

If Equation (26) was satisfied, point C was determined. If not, another point was selected to recalculate until Equation (26) was satisfied. As analyzed above, $y'_c = 0$. y'_c can be given based on the coordinate of C and Equation (16). The thresholding number for y'_c was given as follows:

$$-0.001 < y'_c < 0.001 \quad (27)$$

The values of a and b met the requirements when Equation (27) was satisfied. If not, the value of a and b were changed to recalculate. This process was continued until the function of the suspension cable was determined. The process diagram is shown in Figure 7. The length of section AB of the cable can be calculated according to the determined formula and Equation (25); that is, the actual length of the project after the function was determined.

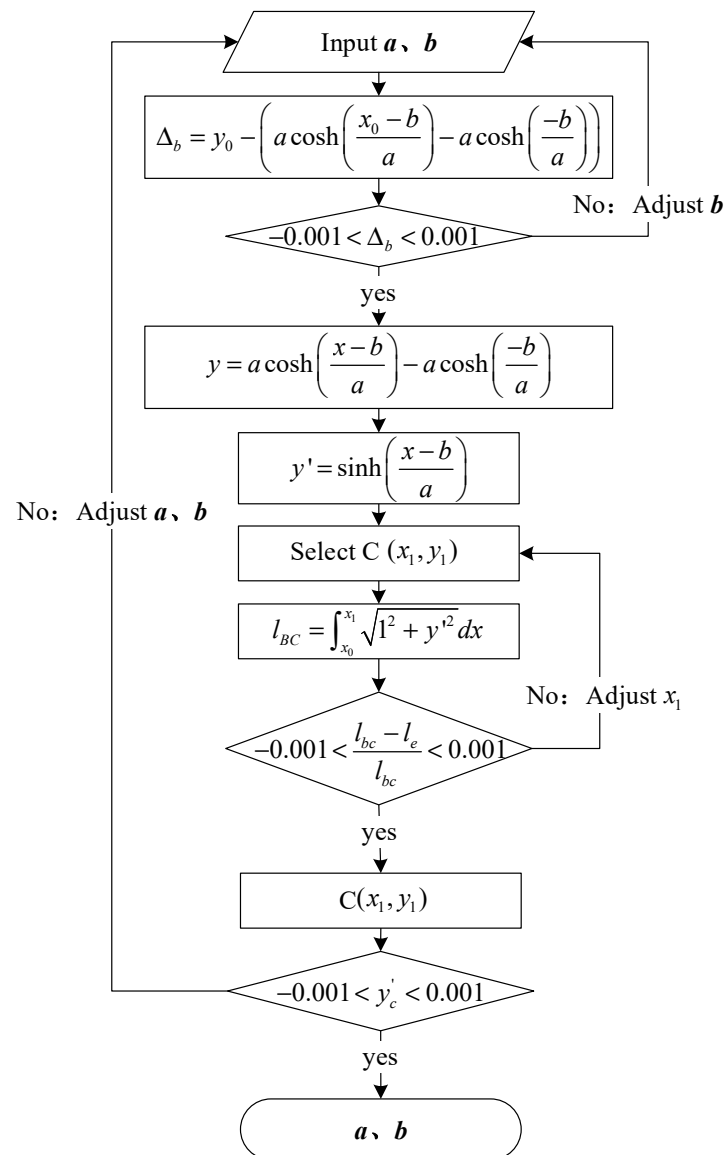


Figure 7. Calculation process of parameters a and b with regard to the function of suspension cable.

Based on an example, the numerical simulation process is demonstrated below.

According to the actual engineering design parameters, the overall span of the suspension cable was 1000 m, and the lowest point of the design was 110 m. The coordinates of point A were (0,0), and the coordinates of point B were (500, -110), which is shown in Figure 8. The length of the equivalent section of insulators and conductors was $l_e = 2175$ m. For point B, the coordinate was (500, -110), which meant the span of the suspension cable was 1000 m, and the lowest of the suspension cable was -110 m. The numerical simulation showed that the requirements were satisfied when $a = 9900$ and $b = 2603.5$. A diagram of the numerical simulation example is shown in Figure 9. Thus, it was calculated that $x_1 = 2655$.

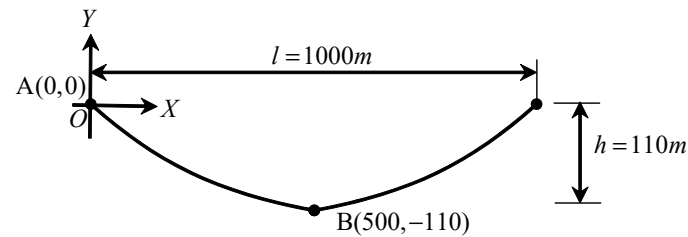


Figure 8. Dimension of long-span CRS.

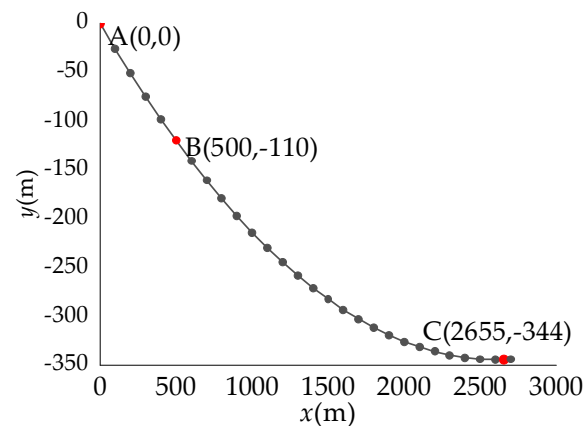


Figure 9. Diagram of solution for numerical simulation example.

In this case, the function was

$$y = 9900 \cosh\left(\frac{x - 2603.5}{9900}\right) - 9900 \cosh\left(\frac{-2603.5}{9900}\right) = 9900 \cosh\left(\frac{x - 2603.5}{9900}\right) - 1024.3 \quad (28)$$

The actual length of the suspension cable, which was also the length of section AB, was as follows:

$$L = \int_0^{500} 9900 \cosh\left(\frac{x - 2603.5}{9900}\right) - 1024.3 = 513.21 \text{ (m)} \quad (29)$$

3. Dynamic Properties Determined by Numerical Analysis

3.1. FE Modeling

The CRS system is a flexible transmission line structural system, and wind-induced structural vibration is critical to its structural safety. The CRS system was composed of cables, which were characterized by small stiffness and large deformation. In practical engineering, the CRS system is mostly used in mountainous areas, where the wind field condition is complex. Due to significant flexibility, there is a huge impact on the structure induced by a complex wind field. Therefore, in the structural simulation analysis of the CRS

system, a reasonable finite element model was indispensable for evaluating its structural performance. For the finite element model, the geometric nonlinearity, which was suitable for a CRS system with significant flexibility, was considered. Also, the finite element model can be used for static analysis while considering static wind load.

As described above, the CRS system was composed of suspension cables, conductors, insulators, and anchorages, while guyed masts and towers were removed. According to the parameters for practical engineering and function analyzed above, coordinates for a suspension cable and conductor were calculated. For the conductor, the initial shape was catenary. For the suspension cable, the initial shape was the approximate equations of suspension cable under the action of a single concentrated force. The suspension cable that hung the suspension insulator was anchored on both ends. The upper end of the insulator was connected to the suspension cable, and the lower end was connected to the conductor. For the conductor, one end was connected to the suspension cable, while another end was anchored. Details on the FE model are given in Figure 10. For a complex flexible structural system, the convergence problem was critical when considering geometrical nonlinearity. This paper adopted an assembly modeling approach. Using this approach, separate analyses of the CRS of the deformed shape and loading states were conducted and finally assembled. All members were modeled by a two-node link element type in three-dimensional space, which meant only tensile force and strain were considered for each element, and the bending and torsion stiffness were ignored [3]. The multiple spans of CRSSI were also modeled and analyzed while considering application to different topographies. The FE model for a multi-span CRSSI is shown in Figure 11.

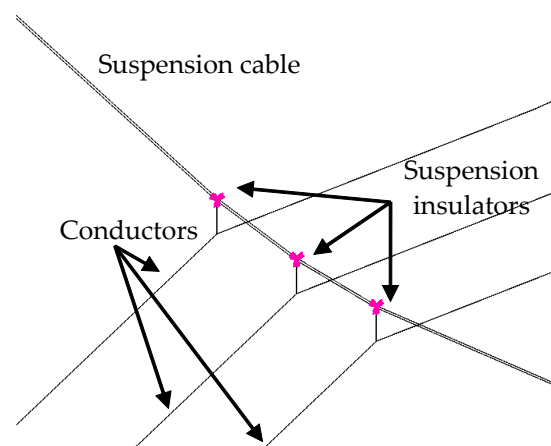


Figure 10. Detail of FE model of long-span CRSSI.

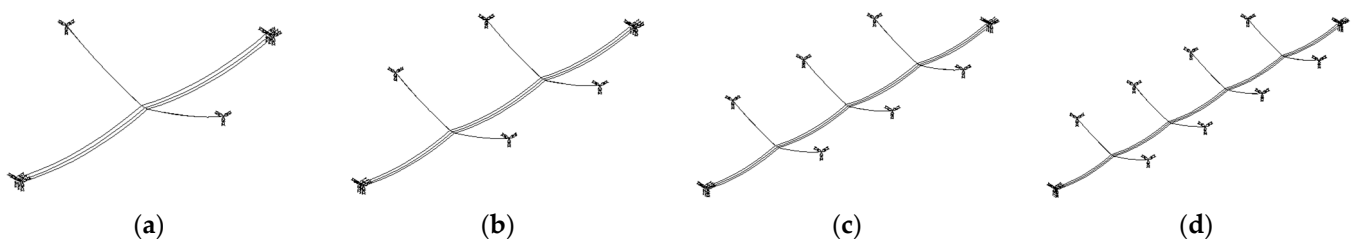


Figure 11. FE models of long-span CRSSI with multiple spans of conductors: (a) 2 spans, (b) 3 spans, (c) 4 spans, (d) 5 spans.

3.2. Dynamic Behavior of CRS

3.2.1. Vibration Modes and Natural Frequencies of Long-Span CRSSI

Firstly, a two-span CRS system was analyzed for modal analysis. The purpose of the modal analysis was to determine the inherent frequency and vibration pattern of the CRS

so as to obtain the vibration characteristics. The modal analyses conducted are shown in Figure 12.

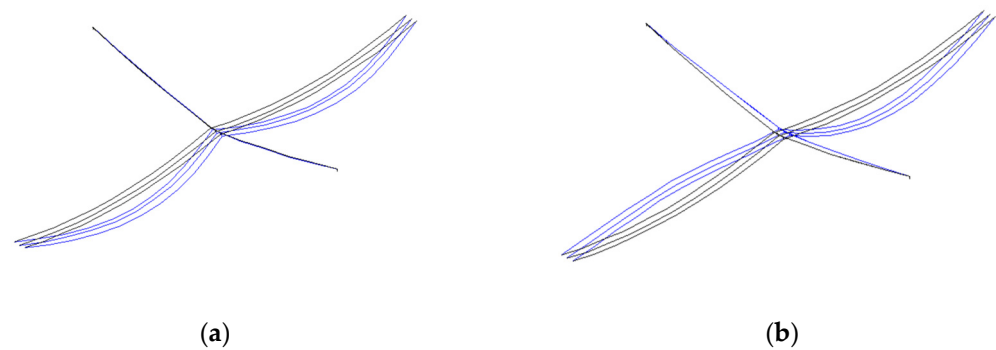


Figure 12. Modal analysis of 2-span CRS system (Black: undeformed, Blue: deformed); (a) 1st symmetric lateral bending (0.0790 Hz); (b) 1st asymmetric vertical bending (0.0813 Hz).

Different numbers of spans were set for the modal analysis of the CRS system. It showed that the frequencies of the same modal for the CRS system were different when considering different numbers of spans. Therefore, the same mode of vibration of the CRS system with different spans should be compared. According to modal calculation results, the frequency of the same mode of vibration decreased as the number of spans increased, as shown in Table 1. The calculated results were plotted on a line graph, as shown in Figure 13. The modes of vibration are shown in Figures 14 and 15. Also, the order of the mode of vibration appearing at different spans was different. At two and three spans, the modes of vibration appeared in the order of the first symmetric lateral bending and the first asymmetric vertical bending. At four and five spans, the orders were the first asymmetric vertical bending and the first symmetric lateral bending. Also, the frequency of the mode of vibration decreased more at the first asymmetric vertical bending. Therefore, it was advised that number of spans selected should be lower than three.

Table 1. Frequency of long-span CRS system at different spans.

Spans	1st Symmetric Lateral Bending (Hz)	1st Asymmetric Vertical Bending (Hz)
2	0.0790	0.0813
3	0.0776	0.0780
4	0.0771	0.0746
5	0.0768	0.0715

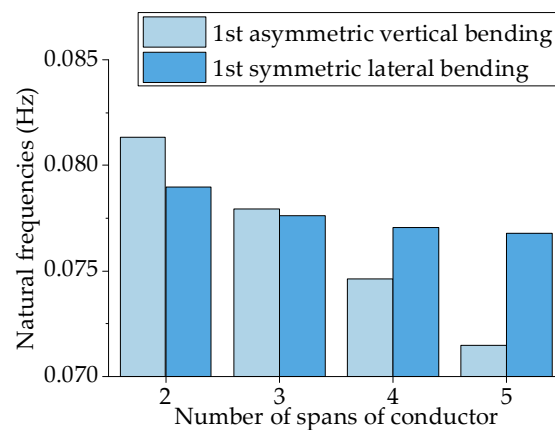


Figure 13. Influence of number of spans on natural frequency.

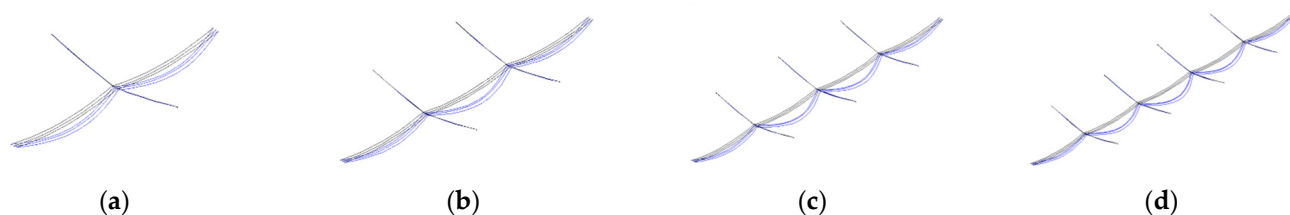


Figure 14. The 1st symmetric lateral bending (Black: undeformed, Blue: deformed): (a) 2 spans, (b) 3 spans, (c) 4 spans, (d) 5 spans.

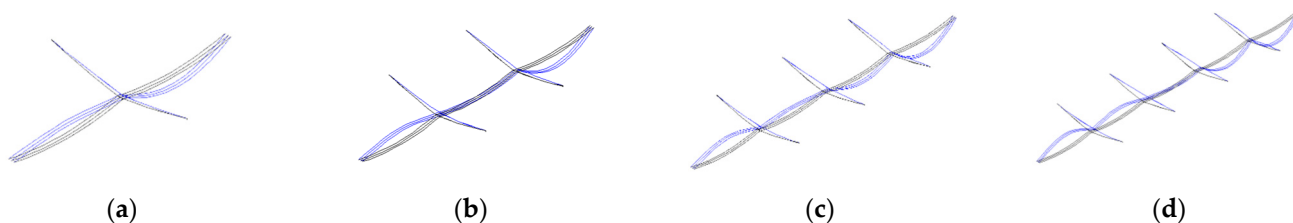


Figure 15. The 1st asymmetric vertical bending (Black: undeformed, Blue: deformed): (a) 2 spans, (b) 3 spans, (c) 4 spans, (d) 5 spans.

3.2.2. Influence of Insulator Structural Parameters on the Dynamic Characteristics of the CRSSI

The type of insulator and the corresponding parameters were different for multiple applications. In the study of dynamic characteristics, the length of insulators should be concerned. Different lengths of the insulators were modified, and the corresponding dynamic characteristics of the CRS system were studied. For insulators, the length of composite insulators used in fouled areas was longer. In areas with hard pollution, the number of pieces of composite insulators was higher, and the total insulator length was 15 m [33]. This chapter focused on the influence of insulator parameters on the dynamic characteristics of the CRS system by modifying the length of the insulator.

Different lengths of SI were set up for the modal analysis of the CRS system. It can be summarized from the calculation results that the natural frequency of the CRS system decreased as the insulator length increased. The reason was that the increment in the length of the SI decreased the stiffness of the structure. Also, with the increase in the number of spans, the impact of the length of the SI on the natural frequency of the structure decreased. The change in the length of the insulator had a small effect on the modal and frequency of the first asymmetric vertical bending but a large influence on the frequency of the first symmetric lateral bending. The calculated results were plotted on a line graph, as shown in Figure 16. For CRSSI, the decrease in the length of the insulator can reduce the natural frequency. For the transmission tower, when the length of the insulator was too small, the conductor and suspension cable were close to each other, which may lead to a danger of discharge. Therefore, an appropriate and safe insulator length should be selected in practical projects when construction.

3.2.3. Comparison of CRSSI and CRSTI

For a CRS system, there are two main types, CRSSI and CRSTI. In order to compare the dynamic characteristics of the two systems, FE models were established. The dynamic characteristics were calculated and summarized for both systems.

FE models were established to calculate the frequency of CRSTI, and a comparison was made between the natural frequency of the same mode of vibration of CRSSI and CRSTI. The natural frequency of each mode of vibration is shown in Table 2. The calculated results were plotted on a line graph, as shown in Figure 17. For the first symmetric lateral bending, the natural frequency of CRSTI was higher than CRSSI in the two spans. The opposite was true when the number of spans was higher than two. For asymmetric vertical bending, the

natural frequency of CRSTI was lower than CRSSI. According to the results, an increase in the number of spans caused a decrease in the stiffness of the structure, which led to a decrease in the natural frequency. The decrease in structural stiffness was not linear. As the number of spans increases, the reduction in structural stiffness decreases with an increase in span. Compared with CRSSI, the decrease in stiffness for CRSTI was more pronounced with an increase in the number of spans. This indicated that CRSTI was more sensitive to the number of spans. In the case of CRSSI, the crossing of conductors at lower frequencies led to structural damage or short circuits in the transmission line, resulting in economic losses. Therefore, in practical construction, the selection of an appropriate system should align with diverse requirements related to topography and engineering considerations.

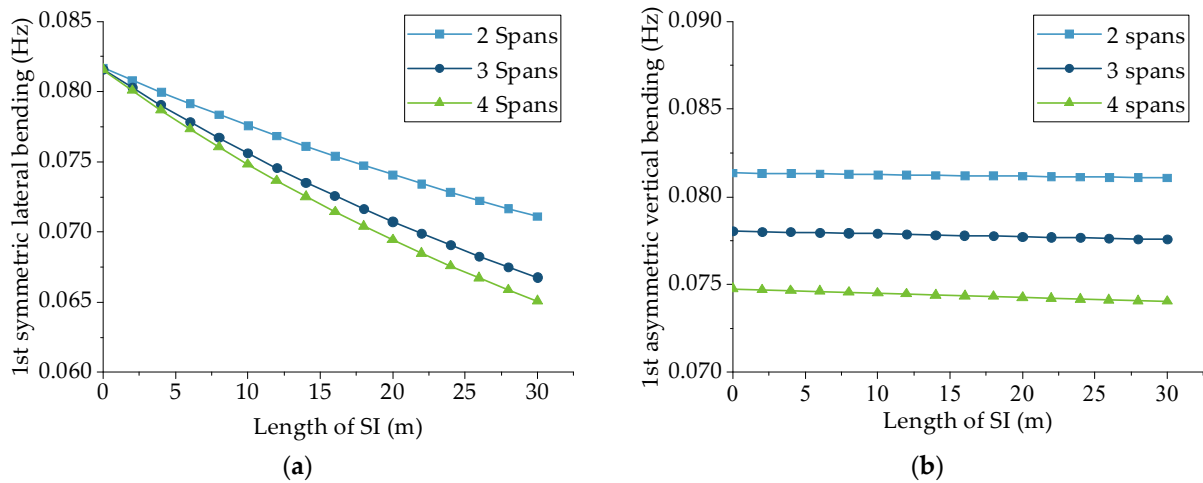


Figure 16. Influence of insulator length on the natural frequency: (a) 1st symmetric lateral bending; (b) 1st asymmetric vertical bending.

Table 2. Comparison of natural frequency between the CRSSI and the CRSTI.

Spans	1st Symmetric Lateral Bending (Hz)			1st Asymmetric Vertical Bending (Hz)		
	CRSTI	CRSSI (SI: 6.42 m)	CRSSI (SI: 12 m)	CRSTI	CRSSI (SI: 6.42 m)	CRSSI (SI: 12 m)
2	0.0818	0.0790	0.0768	0.0653	0.0813	0.0812
3	0.0689	0.0776	0.0746	0.0585	0.0780	0.0779
4	0.0650	0.0771	0.0736	0.0540	0.0746	0.0744

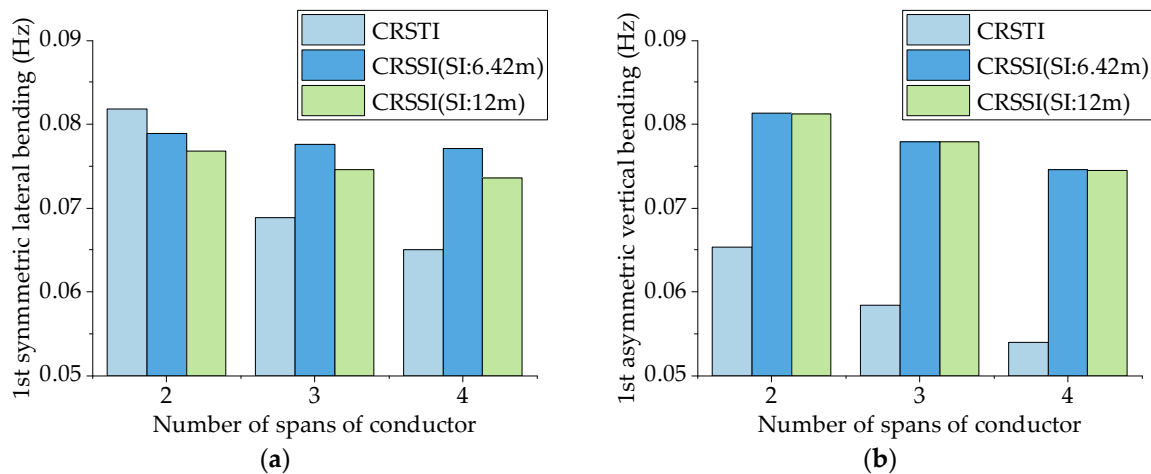


Figure 17. Comparison of natural frequency between CRSSI and CRSTI: (a) 1st symmetric lateral bending; (b) 1st asymmetric vertical bending.

4. Study on Static Wind Load Response for CRSSI

4.1. Calculation of Wind Load

CRS systems with insulators were mainly applied in mountainous areas. The wind load was one of the main external loads that the structure was subjected to. The CRS system with insulator was a wind-sensitive structure. To ensure security, a structural analysis of wind load should be carried out. This chapter focused on the calculation and analysis of the internal force of the suspension cable and the lateral displacement of the conductor for the CRSSI.

Wind loads were considered static wind loads for convenience. According to the wind profile, the average speed of wind in different altitudes was calculated by

$$\bar{v}(z) = \bar{v}_b \left(\frac{z}{z_b} \right)^\alpha \quad (30)$$

where $\bar{v}(z)$ is the average speed of winds in target altitude (m/s), \bar{v}_b is the standard speed of wind (m/s), z is the target altitude (m), and z_b is the standard target altitude (m). α is the ground roughness exponent. Static wind loads can be calculated from a combination of air density, wind speed, windward area, and drag coefficient [34].

It was clear that the windward area was proportional to the wind load. Therefore, the most adverse condition for wind direction was perpendicular to conductors or suspension cables. Wind speeds were calculated for conditions from 0 m/s to 25 m/s. Figure 18 shows a diagram of the structure under wind load.

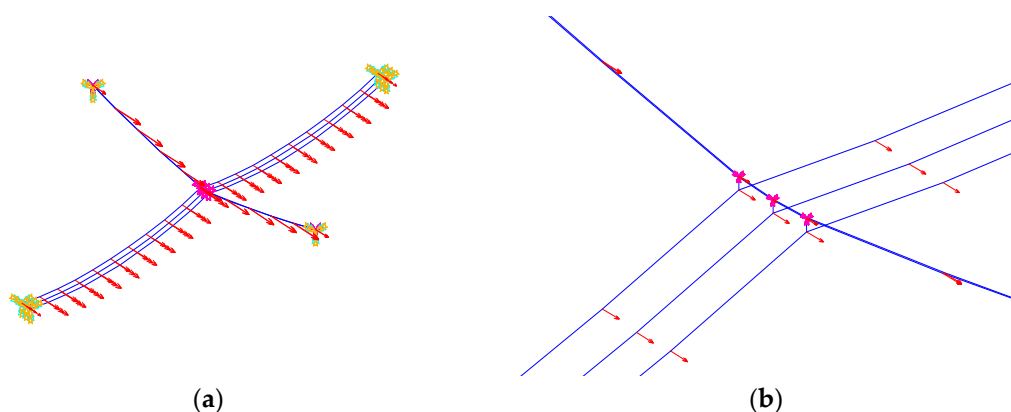


Figure 18. Diagram of wind loading on FE model of 2-span long-span CRS: (a) Fully loaded model; (b) Detail of loaded model.

4.2. Response of Wind Load

As described above, the major concern in static wind load conditions was the internal force and horizontal deformation of the structure. Typical deformation of the long-span CRS under static wind load is shown in Figure 19.

A static wind load was applied to obtain the horizontal displacement of CRSSI. The horizontal displacement of CRSSI was calculated. The length of the suspension insulator was 6.42 m. The displacement of CRSSI was composed of displacement for the insulator, suspension cable, and conductor. In order to analyze the increment in displacement, the displacement of the insulator, suspension cable, and conductor was also calculated. A diagram of different displacements of CRSSI is shown in Figure 20. Moreover, the same calculations were used for CRSSI, in which the length of SI was 0 m in comparison.

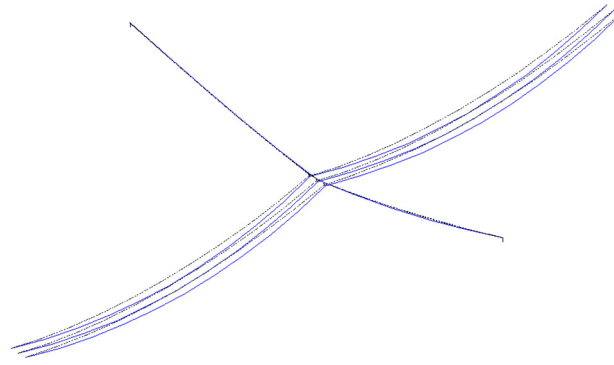


Figure 19. Unscaled deformation of cable-supported structures due to static wind load (Dotted: undeformed, Solid: deformed).

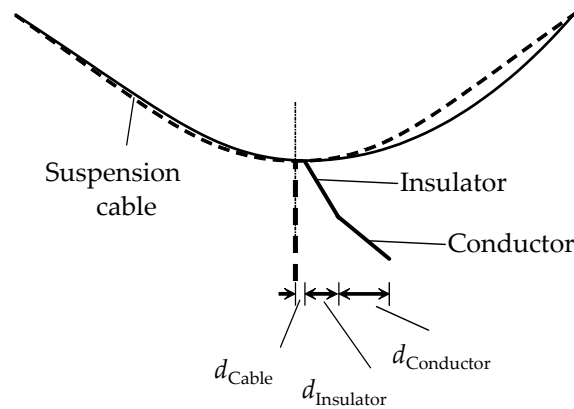


Figure 20. Diagram of displacement of suspension cable of long-span CRSSI (Dotted: undeformed, Solid: deformed, SI = 6.42 m).

As analyzed above, d_{Sum} was calculated:

$$d_{\text{Sum}} = d_{\text{Cable}} + d_{\text{Insulator}} + d_{\text{Conductor}} \quad (31)$$

where d_{Cable} is the displacement of the conductor, $d_{\text{Conductor}}$ is the placement of the conductor, and $d_{\text{Insulator}}$ is the displacement of the insulator. Here, the length of the SI was 6.42 m.

When the length of the SI was 0 m, the displacement of the insulator was 0 m; a diagram of each displacement is shown in Figure 21. As analyzed above, d'_{Sum} was calculated as follows:

$$d'_{\text{Sum}} = d'_{\text{Cable}} + d'_{\text{Conductor}} \quad (32)$$

where d'_{Cable} is the displacement of the conductor, and $d'_{\text{Conductor}}$ is the placement of the conductor. Here, the length of the SI was 0 m.

In Table 3, d_{Cable} is approximately equal to d'_{Cable} , which means the displacement of the suspension cable had a small influence on the increment in displacement. On the contrary, the displacement of the insulator could not be ignored. To analyze the reason for the increment in displacement, Δ_d was calculated:

$$\Delta_d = d_{\text{Sum}} - d'_{\text{Sum}} \quad (33)$$

where d_{Sum} is the horizontal displacement for SI = 6.42 m, and d'_{Sum} is the horizontal displacement for SI = 0 m.

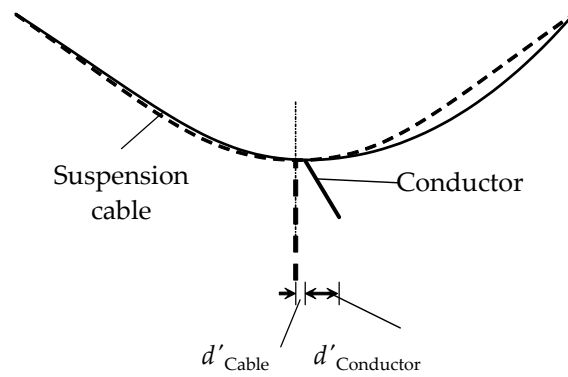


Figure 21. Diagram of displacement of suspension cable of long-span CRSSI (Dotted: undeformed, Solid: deformed, SI = 0 m).

Table 3. Comparison of displacement for SI with length of 6.42 m and length of 0 m.

Wind Speed (m/s)	SI = 6.42 m				SI = 0 m			Δ_d
	d_{Sum}	d_{Cable}	$d_{Insulator}$	$d_{Conductor}$	d'_{Sum}	d'_{Cable}	$d'_{Conductor}$	
0	0.00	0.00	0.00	0.00	0.00	0.00	0.00	0.00
5	0.93	0.01	0.12	0.80	0.87	0.01	0.86	0.06
10	3.73	0.05	0.46	3.22	3.50	0.05	3.45	0.23
15	8.20	0.11	1.01	7.08	7.68	0.11	7.57	0.52
20	14.20	0.20	1.75	12.25	13.29	0.20	13.09	0.91
25	21.00	0.30	2.60	18.10	19.70	0.30	19.40	1.30

d_{Sum} , d'_{Sum} , Δ_d , and $d_{Insulator}$ were plotted as a line graph in Figure 22. Δ_d was approximately half of $d_{Insulator}$. The reason for this was that maximum horizontal displacement for the conductor was at the midpoint of the conductor. The increase in $d_{Insulator}$ increased the displacement of one end for the conductor, while the other end of the conductor did not change. Thus, based on conditions of geometry, the increment of $d_{Conductor}$ was approximately half of $d_{Insulator}$. So, Δ_d was approximately half of $d_{Insulator}$. The larger $d_{Insulator}$ resulted in a larger $d_{Conductor}$, and the horizontal displacement of the CRS system increased. In summary, a longer SI resulted in lower frequency and greater displacement, while a shorter SI posed a risk of discharge and made construction more challenging. Consequently, the length of the SI must be constrained within reasonable limits.

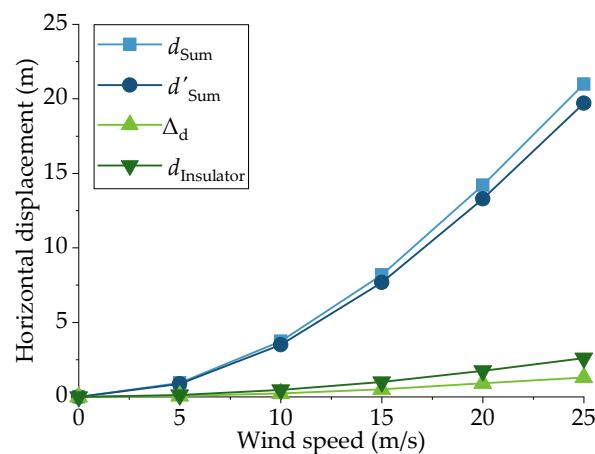


Figure 22. Influence of wind speed on maximum horizontal displacement of conductor.

A static wind load was applied to obtain the horizontal displacement of CRSTI, and a comparison between CRSTI and CRSSI was made. The displacements of the conductor

under different wind speeds for the two systems are shown in Figure 23. It was summarized that horizontal displacements of the conductor were increased with the increase in wind speed in the two systems. Further, the horizontal displacement of CRSSI was higher than that of CRSTI. The reason for this was that under the same condition of wind speed, for CRSSI, the wind load acted not only on the conductor and the cable but also on the insulator. The increment in the displacement caused by the insulator needed to be considered, which led to the displacement of CRSSI being higher. In practical application, an excessive lateral displacement led to a distance between the conductor and the cable that fell below the safe space, posing a risk to the integrity of the transmission structure.

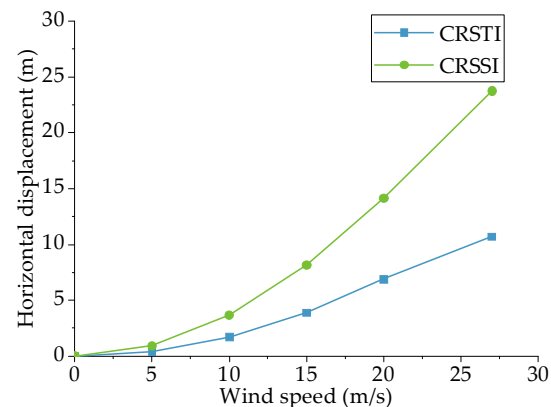


Figure 23. Influence of wind speed on tensile force of suspension cable.

Different numbers of spans were used to study their influence on the tension force of the suspension cable and horizontal displacement. The results are shown in Figure 24. As shown in Figure 24, the increase in the spans had no effect on the tensile force of the suspension cable and the horizontal displacement of the conductor. The same calculation was used for CRSTI, and the results are shown in Figure 25. The calculation results were similar for both systems, and the number of spans had no effect on the two systems. In the case of horizontal displacement, an increase in spans not only raised the wind load on the structure but also added weight to the entire system. As a result, the incremental increase in horizontal displacement could be disregarded for both structures. Regarding tension force, the conductors were connected to insulators or suspension cables, and an increase in span had no influence on the individual conductor, resulting in the constancy of tensile force on both structures.

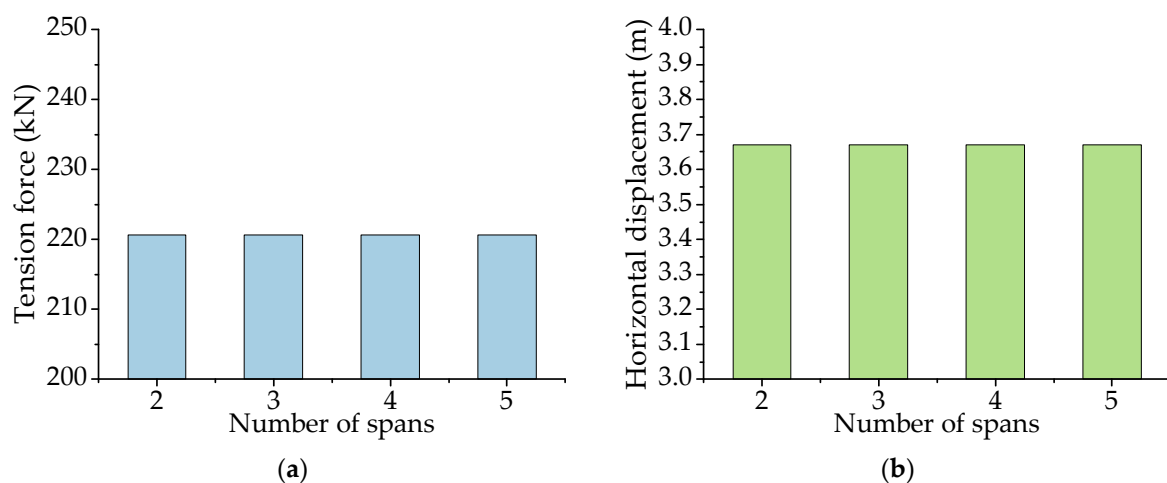


Figure 24. Influence of number of spans of conductor on CRSSI: (a) tensile force of suspension cable (b) horizontal displacement (wind speed = 10 m/s).

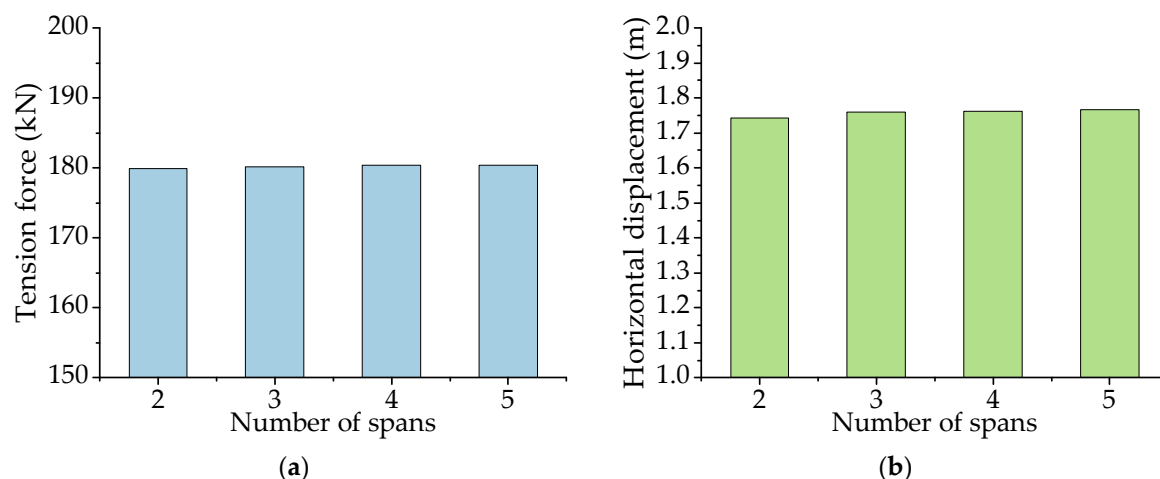


Figure 25. Influence of number of spans of conductor for CRSTI: (a) tensile force of suspension cable (b) horizontal displacement (wind speed = 10 m/s).

5. Conclusions

This paper presents a study of a theoretical modeling approach and FE analysis for long-span CRS with a suspension insulator. The following conclusions were drawn:

- The formula for cables of a long-span CRS system with an insulator and a process of numerical solution were given. Based on classic expression of catenary, the approximate formula of suspension cable under the action of a single concentrated force was derived. A process for numerical solution was given and demonstrated. The presented discussion about the expression of cable was proved to be meaningful for further modeling in FEA. The function of suspension cables and conductors deduced in this paper was applicable to calculate the non-tensional length before construction.
- With an FE model, dynamic properties of a long-span CRS with a suspension insulator were analyzed. The natural frequency of CRSSI decreased with the increase in the number of spans and the length of the SI. Moreover, comparisons between CRSSI and CRSTI were made. With regard to the vibration mode of the first symmetric lateral bending, the natural frequency of CRSTI was higher than that of CRSSI in the two spans. The opposite was true when the number of spans was higher than two. With regard to the mode of vibration of the first asymmetric vertical bending, the natural frequency of CRSTI was lower than that of CRSSI.
- The loading effect of static wind on long-span CRS with a suspension insulator was calculated by means of FEA. Increasing wind speed resulted in an increase in horizontal displacement of the conductor for CRSSI. The number of spans had less influence on the tension of the suspension cable and the horizontal displacement of the conductor. With the same conditions of wind speed, the horizontal displacement of CRSSI was higher than CRSTI.

Author Contributions: Conceptualization, X.T.; Methodology, Q.Q., X.T. and L.Y.; Software, Q.Q., Z.W. and S.H.; Validation, Y.H. and Z.W.; Investigation, S.H.; Resources, L.Y. All authors have read and agreed to the published version of the manuscript.

Funding: The research reported in this paper was conducted with the support of the National Natural Science Foundation of China (Project No. 52178455).

Data Availability Statement: All data are summarized in the tables.

Conflicts of Interest: Author Yujing Hu was employed by the company Design Institute of Chongqing Iron & Steel Group Co., Ltd. Authors Lin Yu and Shengli Hou were employed by the company Chongqing Haizhuang Wind Power Engineering Technology Co., Ltd. The remaining authors declare

that the research was conducted in the absence of any commercial or financial relationships that could be construed as a potential conflict of interest.

References

- Burger, B.A.; Serrano, J.D.; Marais, P.; Jacobs, B. Construction of overhead lines in environmentally sensitive areas. *Transm. Distrib.* **2011**, *3*, 36–43.
- Li, Z.; Hu, Y.; Tu, X. Wind-Induced Response and Its Controlling of Long-Span Cross-Rope Suspension Transmission Line. *Appl. Sci.* **2022**, *12*, 1488. [[CrossRef](#)]
- Tu, X.; Wu, Y.; Li, Z.; Wang, Z. Vortex induced vibration and its controlling of long span Cross-Rope Suspension transmission line with tension insulator. *Struct. Eng. Mech.* **2021**, *78*, 87–102.
- Toklu, Y.C.; Bekdaş, G.; Temur, R. Analysis of cable structures through energy minimization. *Struct. Eng. Mech.* **2017**, *62*, 749–758.
- Jia, Y.; Liu, R. Form-Finding System for Overhead Transmission Line Based on ANSYS. *Energy Procedia* **2012**, *17*, 975–982.
- Peyrot, A.H.; Lee, J.W.; Jensen, H.G.; Osteraas, J.D. Application of Cable Elements Concept to a Transmission Line with Cross Rope Suspension Structures. *IEEE Trans. Power Appar. Syst.* **1981**, *7*, 3254–3262. [[CrossRef](#)]
- Nie, X.; Yan, Z.; Shi, J.; You, Y. The Refined Simulation and Model Analysis of the Suspension Cable Guyed Tower. *J. Shanghai Jiaotong Univ.* **2019**, *53*, 1066–1073.
- Kempner, L., Jr.; Smith, S. Cross-rope Transmission tower-line dynamic analysis. *J. Struct. Eng. ASCE* **1984**, *110*, 1321–1335. [[CrossRef](#)]
- McClure, G.; Lapointe, M. Modeling the structural dynamic response of overhead transmission lines. *Comput. Struct.* **2003**, *81*, 825–834. [[CrossRef](#)]
- Wang, J.; Zhu, S.; Peng, B.; Duan, S.; Li, P. (Eds.) Static and dynamic mechanical characteristic comparison research of v-type insulator string under gale condition. In *IOP Conference Series: Earth and Environmental Science*; IOP Publishing: Bristol, UK, 2017.
- Duan, F.; Song, Y.; Gao, S.; Liu, Y.; Chu, W.; Lu, X.; Liu, Z. Study on aerodynamic instability and galloping response of rail overhead contact line based on wind tunnel tests. *IEEE Trans. Veh. Technol.* **2023**, *72*, 7211–7220. [[CrossRef](#)]
- Zhang, J.; Xie, Q. Failure analysis of transmission tower subjected to strong wind load. *J. Constr. Steel Res.* **2019**, *160*, 271–279. [[CrossRef](#)]
- Zhang, Q.; Popplewell, N.; Shah, A. Galloping of bundle conductor. *J. Sound Vib.* **2000**, *234*, 115–134. [[CrossRef](#)]
- Desai, Y.; Yu, P.; Popplewell, N.; Shah, A. Finite element modelling of transmission line galloping. *Comput. Struct.* **1995**, *57*, 407–420. [[CrossRef](#)]
- Savory, E.; Parke, G.A.; Zeinoddini, M.; Toy, N.; Disney, P. Modelling of tornado and microburst-induced wind loading and failure of a lattice transmission tower. *Eng. Struct.* **2001**, *23*, 365–375. [[CrossRef](#)]
- Song, Y.; Zhang, M.; Øiseth, O.; Rønquist, A. Wind deflection analysis of railway catenary under crosswind based on nonlinear finite element model and wind tunnel test. *Mech. Mach. Theory* **2022**, *168*, 104608. [[CrossRef](#)]
- Chen, T.; Huang, Y.-C.; Xu, Z.-W.; Chen, J.C.Y. Wind vibration control of stay cables using an evolutionary algorithm. *Wind Struct.* **2021**, *32*, 71–80.
- Li, H.N.; Tang, S.Y.; Yi, T.H. Wind-rain-induced vibration test and analytical method of high-voltage transmission tower. *Struct. Eng. Mech.* **2013**, *48*, 435–453. [[CrossRef](#)]
- Vecchiarelli, J. *Aeolian Vibration of a Conductor with a Stockbridge-Type Damper*; University of Toronto: Toronto, ON, Canada, 1997.
- Jafari, M.; Hou, F.; Abdelkefi, A. Wind-induced vibration of structural cables. *Nonlinear Dyn.* **2020**, *100*, 351–421. [[CrossRef](#)]
- Martins, A.M.; Simões, L.M.; Negrão, J.H. Optimization of cable-stayed bridges: A literature survey. *Adv. Eng. Softw.* **2020**, *149*, 102829. [[CrossRef](#)]
- Liu, Z.; Song, Y.; Gao, S.; Wang, H. Review of Perspectives on Pantograph-Catenary Interaction Research for High-Speed Railways Operating at 400 km/h and above. *IEEE Trans. Transp. Electr.* **2023**. [[CrossRef](#)]
- Yin, X.; Shi, Y.; Xu, X.; Duan, Y.; Jia, Y.; Chen, G.; Zhang, X.; Yin, F. (Eds.) Research on Wind Deviation Detection Based on DENCLUE Abnormal Working Condition Filtering. In *IOP Conference Series: Earth and Environmental Science*; IOP Publishing: Bristol, UK, 2020.
- Okamura, T.; Ohkuma, T.; Hongo, E.; Okada, H. Wind response analysis of a transmission tower in a mountainous area. *J. Wind Eng. Ind. Aerodyn.* **2003**, *91*, 53–63. [[CrossRef](#)]
- Keyhan, H.; McClure, G.; Habashi, W.G. Dynamic analysis of an overhead transmission line subject to gusty wind loading predicted by wind-conductor interaction. *Comput. Struct.* **2013**, *122*, 135–144. [[CrossRef](#)]
- Lalonde, S.; Guilbault, R.; Langlois, S. Modeling multilayered wire strands, a strategy based on 3D finite element beam-to-beam contacts—Part II: Application to wind-induced vibration and fatigue analysis of overhead conductors. *Int. J. Mech. Sci.* **2017**, *126*, 297–307. [[CrossRef](#)]
- Jia, J. (Ed.) Wind induced dynamic response and fatigue assessment—Nonlinear time domain versus linear stochastic analysis. In *Structures*; Elsevier: Amsterdam, The Netherlands, 2021.
- Deng, H.; Xu, H.; Duan, C.; Jin, X.; Wang, Z. Experimental and numerical study on the responses of a transmission tower to skew incident winds. *J. Wind Eng. Ind. Aerodyn.* **2016**, *157*, 171–188. [[CrossRef](#)]
- Pombo, J.; Ambrósio, J. Environmental and track perturbations on multiple pantograph interaction with catenaries in high-speed trains. *Comput. Struct.* **2013**, *124*, 88–101. [[CrossRef](#)]

30. Pombo, J.; Ambrósio, J.; Pereira, M.; Rauter, F.; Collina, A.; Facchinetti, A. Influence of the aerodynamic forces on the pantograph–catenary system for high-speed trains. *Veh. Syst. Dyn.* **2009**, *47*, 1327–1347. [[CrossRef](#)]
31. Stickland, M.; Scanlon, T.; Craighead, I.; Fernandez, J. An investigation into the mechanical damping characteristics of catenary contact wires and their effect on aerodynamic galloping instability. *Proc. Inst. Mech. Eng. Part F J. Rail Rapid Transit.* **2003**, *217*, 63–71. [[CrossRef](#)]
32. Song, Y.; Liu, Z.; Rønnquist, A.; Nåvik, P.; Liu, Z. Contact wire irregularity stochastics and effect on high-speed railway pantograph–catenary interactions. *IEEE Trans. Instrum. Meas.* **2020**, *69*, 8196–8206. [[CrossRef](#)]
33. Xu, J. Wet Snow Flashover Characteristics of 500-kV AC Insulator Strings with Different Arrangements. *Appl. Sci.* **2019**, *9*, 930. [[CrossRef](#)]
34. Yan, Z.; Li, Z.; Savory, E.; Lin, W.E. Galloping of a single iced conductor based on curved-beam theory. *J. Wind Eng. Ind. Aerodyn.* **2013**, *123*, 77–87. [[CrossRef](#)]

Disclaimer/Publisher’s Note: The statements, opinions and data contained in all publications are solely those of the individual author(s) and contributor(s) and not of MDPI and/or the editor(s). MDPI and/or the editor(s) disclaim responsibility for any injury to people or property resulting from any ideas, methods, instructions or products referred to in the content.